Tree Physiology 40, 1697–1711
doi:10.1093/treephys/tpaa087

Research paper

Tree physiological monitoring of the 2018 larch budmoth outbreak: preference for leaf recovery and carbon storage over stem wood formation in *Larix decidua*

Richard L. Peters[1,2,8], Jose Carlos Miranda[1,3], Leonie Schönbeck[1], Daniel Nievergelt[1], Marina V. Fonti[1,4], Matthias Saurer[1], Ana Stritih[5,6], Patrick Fonti[1], Beat Wermelinger[7], Georg von Arx[1] and Marco M. Lehmann[1]

[1]Forest Dynamics, Swiss Federal Research Institute for Forest, Snow and Landscape Research (WSL), Zürcherstrasse 111, Birmensdorf CH-8903, Switzerland; [2]Department of Plants and Crops, Faculty of Bioscience Engineering, Laboratory of Plant Ecology, Ghent University, Coupure links 653, Ghent B-9000, Belgium; [3]Forest Genetics and Ecophysiology Research Group, School of Forestry Engineering, Universidad Politécnica de Madrid, Ciudad Universitaria s/n, Madrid 28040, Spain; [4]Institute of Ecology and Geography, Siberian Federal University, 79 Svobodny pr., Krasnoyarsk 660041, Russia; [5]ETH Zurich, Institute for Landscape and Spatial Development, Planning of Landscape and Urban Systems (PLUS), Stefano-Franscini Platz 5, Zürich 8093, Switzerland; [6]WSL Institute for Snow and Avalanche Research SLF, Flüelastrasse 11, Davos Dorf 7260, Switzerland; [7]Forest Health and Biotic Interactions, Swiss Federal Research Institute for Forest, Snow and Landscape Research (WSL), Zürcherstrasse 111, Birmensdorf CH-8903, Switzerland; [8]Corresponding author (richard.peters@wsl.ch)

Received November 24, 2019; accepted July 6, 2020; handling Editor Peter Millard

Insect defoliation impacts forest productivity worldwide, highlighting the relevance of plant–insect interactions. The larch budmoth (*Zeiraphera griseana* Hübner) is one of the most extensively studied defoliators, where numerous tree ring-based analyses on its host (*Larix decidua* Mill.) have aided in identifying outbreak dynamics over the past millennia. Yet, outbreaks have been widely absent after the early 1980s, and little is known about the in situ tree physiological responses and the allocation of carbon resources during and after defoliation. In summer 2018, we tracked an ongoing larch budmoth outbreak in a well-studied larch forest in the Swiss Alps. We performed biweekly monitoring on an affected and unaffected site using a unique combination of xylogenesis observations, measurements of non-structural carbohydrates, isotopic analysis of needle assimilates and ground-based and remote-sensed leaf trait observations. The budmoth induced a defoliation that lasted 40 days and could be detected by satellite observations. Soluble sugars significantly decreased in needles and stem phloem of the defoliated trees, while starch levels remained stable in the stem and root xylem compared to the control. Carbon and oxygen isotope ratios in needle assimilates indicated that neither photosynthetic assimilation rates nor stomatal conductance was different between sites before, during and after the outbreak. Defoliated trees ceased cell wall thickening 17 days earlier than unaffected trees, showing the earliest halt of ring formation recorded from 2007 untill 2013 and causing significant thinner cell walls, particularly in the latewood. No significant differences were found for cell enlargement rates and ring width. Our study revealed that an outbreak causes a downregulation of cell wall thickening first, while no starch is mobilized or leaf physiology is adjusted to compensate for the reduced carbon source due to defoliation. Our observations suggest that affected larch trees prioritize leaf recovery and carbon storage over wood biomass development.

Keywords: cell wall thickness, European Alps, insect outbreak, non-structural carbohydrates (NSC), stable isotopes, tree rings, wood formation, *Zeiraphera griseana*.

Introduction

The evolutionary 'arms race' between plants and insects has resulted in a wide variety of impacts on the host and subsequent plant physiological adaptations (Giron et al. 2018, Pureswaran et al. 2018). Within forests, defoliating insects present a prominent biotic stressor that can negatively impact tree vitality and forest resilience to climate change (McDowell et al. 2008, Galiano et al. 2011, Poyatos et al. 2013, Anderegg et al. 2015, Foster 2017). The larch budmoth (*Zeiraphera griseana* Hübner) is such a defoliator, causing waves of extensive defoliation of its host, the European larch (*Larix decidua* Mill.), across the European alpine arch from west to east (Baltensweiler and Rubli 1999, Johnson et al. 2004). Such outbreaks have been part of these forest ecosystems for millennia, following ~9-year cycles (Baltensweiler and Fischlin 1988, Turchin et al. 2003, Esper et al. 2007). Yet, after the early 1980s, they have been absent over most of the Alps, attributed to changes in forest structure, species composition or environmental conditions (e.g., Asshoff and Hättenschwiler 2006, Johnson et al. 2010, Battipaglia et al. 2014, Iyengar et al. 2016). However, it needs to be stressed that the population cycling continued with the same frequencies of minima and maxima as before, but without causing visible defoliation (Wermelinger et al. 2018). The missing outbreaks have halted further investigations of tree physiological responses and adaptations to larch budmoth outbreaks. Remarkably, in 2016 a new outbreak wave, causing evident defoliation, started in France and reached western Switzerland in 2017. In 2018 widespread larch budmoth outbreaks were observed in several alpine valleys in Switzerland, which provided a unique opportunity to study the direct tree physiological responses of *L. decidua* to larch budmoth larval feeding.

The larch tree–larch budmoth interactions are complex. During an outbreak, large quantities of larvae hatch in spring which feed on the needle clusters and cause visible defoliation. The host's crown foliage can be affected for up to 3 years after the first outbreak year (Baltensweiler and Rubli 1999, Baltensweiler et al. 2008). Larch is however not defenseless and responds by reducing foliage mass and nutritional quality for the defoliator (Benz 1974, Baltensweiler and Fischlin 1988, Asshoff and Hättenschwiler 2006). After a defoliation, larch is able to reflush its foliage within 3–4 weeks after the end of larval feeding, highlighting the resilience to this stressor (Baltensweiler et al. 2008). Such defoliations have most notably caused alterations of the wood structure, generating typical narrow annual tree rings with latewood tracheids showing thin latewood cell walls (Rolland et al. 2001, Esper et al. 2007). This impact on the wood structure is so severe and unambiguous that these 'budmoth rings' have been commonly used to identify past outbreak events (Büntgen et al. 2009, Hartl-Meier et al. 2017, Arbellay et al. 2018). Moreover, in high-elevation forests, these outbreaks show great relevance as they have a stronger impact on biomass accumulation than climate, with the absence of outbreaks since the 1980s causing substantial increases in growth rates (Peters et al. 2017, Weigt et al. 2018). Yet, the impact of defoliation by larch budmoth outbreaks on tree carbon dynamics depends on physiological responses of the host, which still are poorly understood (e.g., Medvigy et al. 2012).

Almost all knowledge on physiological responses to sudden defoliation comes from experimentally induced defoliations on small trees (but see Li et al. 2002), measuring the response in various plant organs. Remaining leaves appear to alter their functioning after a defoliation, i.e., artificially defoliated *Pinus radiata* (5–9–years old) compensated for foliage loss by temporarily increasing the photosynthetic capacity (Eyles et al. 2011; see also Reich et al. 1993). Yet, the capability to alter photosynthetic performance appeared to be species specific (Gleason and Ares 2004, Piper and Fajardo 2014). For instance, for mature *L. decidua*, oxygen ($\delta^{18}O$) and carbon isotopic ($\delta^{13}C$) ratios in tree rings during outbreaks occurring between 1900 and 2004 seemed largely unaffected (Kress et al. 2009; also found for *Abies balsamea* in Simard et al. 2012), suggesting similar stomatal conductance and photosynthetic capacity (see Scheidegger et al. 2000). Ambiguous results were also found for non-structural carbohydrates (NSC; including starch, sucrose, glucose and fructose) among different tree organs and species. While 100% defoliation caused a significant depletion of NSC levels in roots of treeline *Pinus cembra* (Li et al. 2002), studies on other species revealed only a short-term and limited impact on the NSC pools in different tree organs (e.g., needles, branches and roots; see Puri et al. 2015 studying *Pinus pinaster*), likely because trees prioritize carbon storage over structural carbon investment (Wiley et al. 2013, Jacquet et al. 2014). The removal of available carbon due to defoliation can also substantially downregulate wood biomass formation (Schmid et al. 2017, Castagneri et al. 2020) and has severe implications for the wood structure, where defoliation can reduce xylem cavitation resistance, due to thinner and less lignified cell walls, and phloem transport efficiency, due to smaller and more irregular-shaped phloem sieve tubes (Hillabrand et al. 2019). Among the few studies focussing on mature trees, Wiley et al. (2016) showed that defoliation strongly downregulates growth for 3 years while prioritizing re-foliation and NSC storage and maintaining the reproduction cycle (see also Puri et al. 2015). Unfortunately, these studies can only provide hypotheses about the potential regulating mechanisms, which have yet to be confirmed with in situ physiological measurement during a naturally occurring larch budmoth outbreak.

Defoliation after a larch budmoth outbreak requires *L. decidua* to invest carbon into building new foliage. The lower carbon availability during de- and re-foliation likely affects the formation of wood by the secondary meristem (the cambium) and the

resulting wood structure. Budmoth rings are produced due to alterations in wood formation kinetics, including duration and rate of cambial cell division, cell growth and cell wall thickening (Cuny et al. 2014). Cell wall thickening has been shown to have different kinetics than cell elongation (Cuny et al. 2015), yet is still impacted by the availability of NSC (Rathgeber et al. 2016, Friend et al. 2019). Moreover, wood cell production and elongation, which determine ring width, are influenced by the turgor pressure in the cambium, hormone gradients and the concentration of NSC (De Schepper and Steppe 2010, Simard et al. 2013, Hartmann et al. 2017). These wood formation processes are likely hampered during a defoliation event and cause the production of fewer tracheids with thinner latewood cell walls (Castagneri et al. 2020), yet no wood formation observations are available to validate these assumptions. Thus, despite the fact that the resulting ring width structure has been used for decades to reconstruct larch budmoth outbreak dynamics (e.g., Rolland et al. 2001), the underlying physiological mechanisms remain unclear.

Therefore, the question remains of how defoliation during a larch budmoth outbreak affects the physiology of the needles and how this cascades to the NSC concentrations within different tree organs and subsequently affects the wood formation processes. This short-term reduction of carbon assimilation due to the defoliation is important as it alters the carbon input of mature trees growing under natural conditions (e.g., Rademacher et al. 2019). Based on these considerations, we thus establish two contrasting hypotheses on the mechanism behind the observed reduction in secondary growth and its subsequent carbon allocation. One logical hypothesis (H1) is that the temporary lack of carbon, due to the reduced leaf area, is actively compensated by increasing photosynthetic capacity of the new foliage. The overcompensation stabilizes the NSC concentration in various tree organs to ensure long-term survival while discriminating against wood formation processes (see Schmid et al. 2017). Conversely, hypothesis (H2) postulates that the leaf physiology of re-foliated needles stays unaltered, causing a lower availability of NSC concentrations in tree organs (e.g., twigs, stem and roots), and subsequently retards wood formation, as the lower availability of carbon resources reduces osmotic potential needed for turgor-driven cell elongation and resources to sustain cell wall thickening. This passive response would then show a subsequent reduction of NSC in storage tissues (e.g., stem xylem, root xylem) as these pools are not replenished (see Li et al. 2002).

Here we performed a unique (bi)weekly physiological monitoring of mature *L. decidua* trees exposed to the first intense larch budmoth outbreak reported since the early 1980s. The study was conducted in a well-monitored high-elevation forest in the western Swiss Alps in 2018 (see King et al. 2013, Simard et al. 2013, Cuny et al. 2019, Peters et al. 2019), where (bi)weekly samples from multiple tissues (leaves, twig xylem, stem xylem, stem phloem and root xylem) were collected over the entire growing season on an affected and unaffected site. A unique combination of xylogenesis observations, NSC analysis, leaf trait measurements and carbon and oxygen analyses were performed to track wood formation, carbon allocation dynamics and leaf physiological performance. We expect H1 to be true, where the defoliation by the larch budmoth influences (i) the source-to-sink carbon allocation strategies, (ii) the functionality of needles before and after the outbreak and (iii) the temporal dynamics of wood formation and wood anatomy. This study is among the first to perform multiple physiological measurements during an ongoing insect outbreak event and contributes to refining the understanding of mechanisms behind the impact of reduced carbon assimilation on tree physiology and wood production in mature trees.

Materials and methods

Study site

The study area is located in the Lötschental valley of the Swiss Alps (46°23′40″N, 7°45′35″E; Figure 1a). The valley is largely covered by forest, composed of well-mixed populations of Norway spruce and European larch, spanning from the valley bottom at 1300 m above sea level until 2200 m a.s.l. at the treeline (see Peters et al. 2017 for a detailed site description). In this valley at least nine budmoth outbreaks occurred since 1900 (Peters et al. 2017, Büntgen et al. 2020). Mean annual total precipitation in the valley is 800 mm with mean annual air temperature of ~5 °C. The valley was selected due to the presence of outbreak and past intensive monitoring along an elevational transect (King et al. 2013, Simard et al. 2013, Peters et al. 2019). Particularly the data from a nearby site from Cuny et al. (2019), indicated as the 'literature' site at 1900 m a.s.l. on the south facing slope in Figure 1a, was used to provide reference environmental measurements, wood formation monitoring and wood anatomical structure analyses spanning the period from 2007 to 2013. The site where the larch budmoth outbreak was observed (hence referred to as 'budmoth site') is located at the upper end of the optimal outbreak elevation (2000 m a.s.l.; Baltensweiler et al. 2008). A second site at a slightly lower elevation (1780 m a.s.l.; the 'control site') was established to provide a control under conditions not affected by budmoth outbreak. The mean age of mature *L. decidua* trees at these elevations is around 200 years (as reported by Peters et al. 2017 and Cuny et al. 2019). At both sites, air temperature (T_a) and relative humidity (RH) were monitored (using a Temperature/RH Sensor Data Logger with a temporal resolution of 10 minutes; Onset, USA, MX2302A; Figure 1b). The forest composition at both sites is similar, with *L. decidua* dominating (Figure 1c), while stand density and tree height were lower at the budmoth site (Table 1). At each site, four dominant and mature *L. decidua* trees were selected for

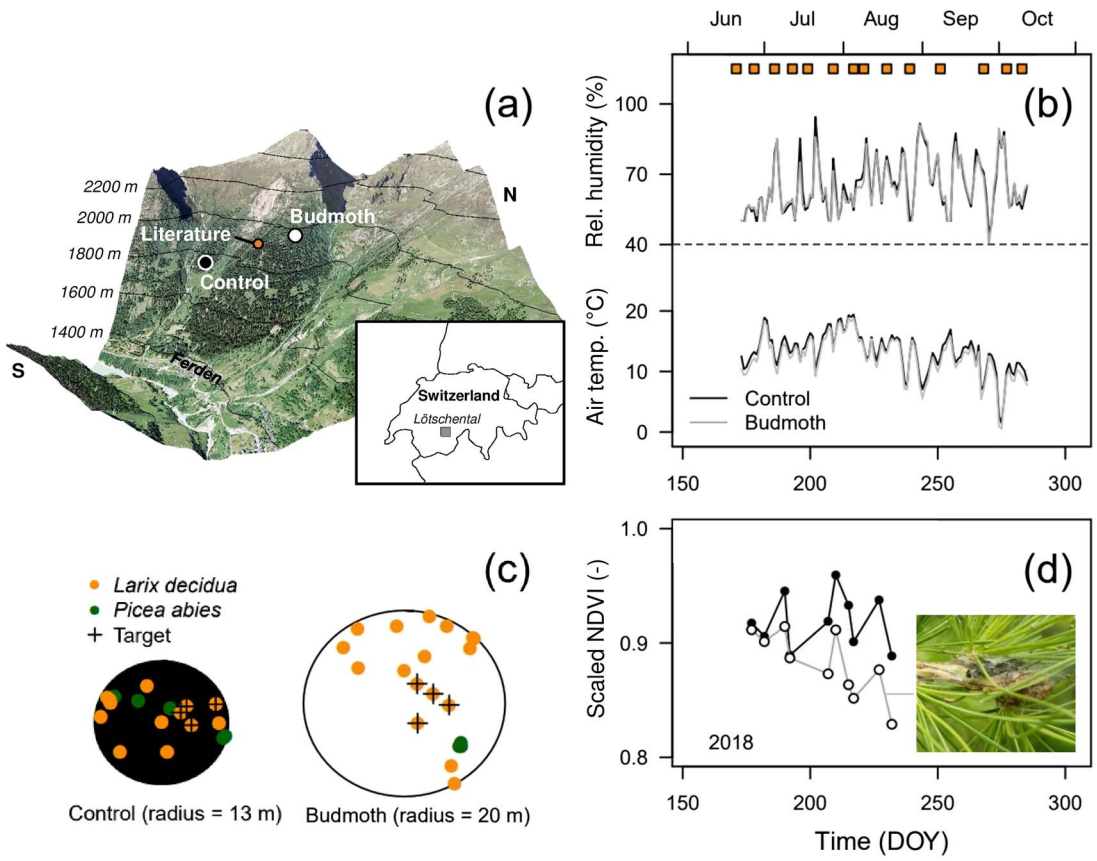

Figure 1. Sampling locations, experimental design and site characteristics. (a) Map of the Lötschental valley in Switzerland with an affected (budmoth, in white) and unaffected (control, in black) site from June to October. Additionally, data from literature on wood formation observation and wood anatomical information at a nearby site at 1900 m a.s.l., spanning the period from 2007 to 2013, was included (see Cuny et al. 2019; literature; in orange). (b) Daily mean relative humidity and air temperature time series for the control (in black) and budmoth (in gray) site. Orange squares indicate the days of sampling. (c) Forest composition for both sites in a circular plot with a specified radius. Both *Larix decidua* and *Picea abies* trees are indicated, while the monitored *L. decidua* trees are highlighted (see target). (d) The normalized difference vegetation index (NDVI) time series obtained from satellite images for 2018 (from July till August) against day of the year (DOY), scaled to the maximum NDVI value measured in the period from 2017 to 2018. The inset picture shows a *Zeiraphera griseana* larvae feeding on young *L. decidua* needles.

continuous monitoring (Figure 1b). For each of the eight trees, we recorded social status, position, height of the tree and its crown base (using a Vertex IV, Haglöf Sweden) and diameter at breast height (DBH; Figure 1c; Table 1).

Outbreak and sampling schedule

The sampling period started on the 20 June 2018 (DOY 171), when the larch budmoth outbreak was still at its early stage (i.e., limited visible feeding damage by young larvae; Table 2). Defoliation became clearly visible at the end of June (DOY 178) and reached its maximum at the beginning of July (DOY 186), with little difference in timing between trees. Re-foliation started in mid-July (DOY 193), and all buds were fully re-foliated at the end of July (DOY 209). At the beginning of August (DOY 217), only fully grown mature needles were visible. Thus, the defoliation effect by the larch budmoth lasted for about 40 days (DOY 178 to 217). Further samples were taken until the end of the growing season on 10 October 2018 (DOY 283). All samples were consistently taken between 11:00 and 16:00 on each sampling day. Additionally, on 9 August 2018 (DOY 221), one larger sun-exposed branch per tree was collected, where we randomly selected recent year twigs, transferred them to black plastic bags for transport and stored them in the fridge in the laboratory for leaf trait analyses.

Sun-exposed needle and twig xylem samples were taken with a pole pruner at around 7 m height. Stem phloem (visually distinct from the xylem and dead bark due to a distinct coloration) and xylem (only sapwood) were collected with a 1 cm diameter increment borer (Haglöf, Sweden). Coarse root xylem was collected by digging out large accessible roots with a diameter of around 5–7 cm and chiseling out a 2 × 3 cm piece. Root sapwood samples were collected approximately once per month to minimize damage. All samples were transferred into gas-tight 12 mL glass vials (Exetainer, Labco, Lampeter, UK), stored in cooling bags with ice packs and afterwards frozen for NSC and stable isotope analyses. Water was then cryogenically extracted from needles and stem xylem using a vacuum distillation line (Lehmann et al. 2018). Samples of twig xylem, stem phloem,

Table 1. Main characteristics of sites and target trees.

Site	Lat. °N	Lon. °E	Elev. (m a.s.l.)	Stand density (trees ha^{-1})	Tree	DBH[1] (cm)	Height (m)	Crown base (m)	Defoliation (%)
Control	46.39475	7.74626	1780	339	C1	55	27.7	9.1	0
					C2	60	26.5	7.5	0
					C3	76.5	27.4	6.9	0
					C4	49.3	26.8	11	0
						60 ± 12	27 ± 1	9 ± 2	
Budmoth	46.39922	7.74656	2000	167	D1	81.5	16.9	3.7	80
					D2	42.2	14.8	4	60
					D3	36.8	16.8	5	60
					D4	40.4	18.4	5.1	40
						50 ± 21	17 ± 2	5 ± 1	

[1]DBH, diameter at breast height (1.3 m).

Table 2. Outbreak and sampling schedule. For each tissue type, the DOY is provided. The gray area indicates the period when trees showed visual damage from the outbreak.

			June		July				August				September			
Method	Tissue	DOY	171[1]	178	186	193	199	209	217	221	230	239	251	268	277	283
XYL[2]	Stem xylem		X	X	X	X	X	X	X	X	X	X	X	X	X	X
NSC[3]/ISO[4]	Needles		X	X	X	X	X					X				X
NSC	Twig xylem															
NSC	Stem phloem		X		X	X	X					X				X
NSC/ISO	Stem xylem															
NSC	Root xylem		X				X					X				X
Budmoth damage				Defoliation	Max defoliation	Refoliating			Mature leaves							

[1]The budmoth plot was first sampled on DOY 171 and control plot on DOY 172.
[2]XYL, xylogenesis.
[3]NSC, non-structural carbohydrates.
[4]ISO, isotopic analyses of needle assimilates and stem xylem water.

stem xylem and root xylem were oven-dried at 70 °C. All samples were ground to powder in a steel ball mill for further analysis.

In addition, microcores were collected at breast height on the stem using a Trephor (Rossi et al. 2006) and stored in ethanol to monitor xylogenesis at 4 to 17 days interval. At the end of the 2018 growing season, a wood increment core was taken from each tree to analyze the wood anatomical structure.

Defoliation analyses and needle trait measurements

To track the defoliation patterns, we studied time series of satellite images and performed on-site evaluations of the needle traits and visually estimated defoliation of the crown area. We downloaded all cloud-free Sentinel-2 Level-2A (atmospherically corrected) images of the Lötschental for the growing seasons of 2017 and 2018 (European Space Agency). The normalized difference vegetation index (NDVI = [Near-infrared − Red]/[Near-infrared + Red]) of the study region was calculated at a 10-m resolution, and the mean value and standard deviation of pixels within the budmoth and control plots were extracted. To compare both sites while accounting for absolute productivity differences, we scaled the NDVI values to the maximum reached at each site during the growing season of 2017.

Needles from the whole branch sample (collected at DOY 221, so after full maturation of the new needles) were used to analyze needle leaf area (LA) using a leaf area meter (LI-3100C, LI-COR, Lincoln, NE, USA). Dry weight (d.w.) of the needle material was determined after oven drying at 70 °C and needle length. The specific leaf area (SLA in $m^2\ kg^{-1}$) is calculated as SLA = LA/d.w. The carbon/nitrogen (C/N) ratio, before (DOY 171) and after (DOY 283) the larch budmoth outbreak, was determined from 1 mg of weekly collected needle organic matter using an EA (EA1110 elemental analyzer, CE Instruments, Milan, Italy) coupled to an IRMS (DeltaPlusXP, Thermo Fisher Scientific).

Analyses of non-structural carbohydrates (NSC)

Non-structural carbohydrates concentrations, reflecting low molecular weight sugars (glucose, fructose and sucrose) and starch, in needles, twig xylem, stem phloem, stem xylem and root xylem were determined using 10–12 mg of ground material, following the protocol as described in (Schönbeck et al. 2018), see also (Hoch et al. 2002). The total amount of soluble sugars was quantified photometrically at 340 nm in a 96-well microplate photometer (HR 7000, Hamilton, Reno, NE, USA) after enzymatic conversion to gluconate-6-phosphate (hexokinase reaction, hexokinase from Sigma Diagnostics, St. Louis, MO, USA). The total amount of NSC was determined by taking 500 µL of the extract (including sugars and starch) incubated (for 15 h at 49 °C) with a fungal amyloglucosidase from *Aspergillus niger* (Sigma-Aldrich, St. Louis, MO, USA) to digest starch into glucose and quantify the total amount photometrically. Pure starch and glucose, fructose and sucrose solutions were used as standards, as well as leaf material with a known NSC concentration (Orchard leaves, Leco, St. Joseph, MI, USA). Soluble sugars and starch concentration values were standardized by dividing all values by their average per plot in the first sampling date ($[Ss_{std}]$ and $[St_{std}]$ respectively; see Table S1 available as Supplementary Data at *Tree Physiology* Online), in order to correct for absolute differences in NSC concentrations between sites before the outbreak and focus on differences in temporal dynamics.

Isotope analysis of source water and needle assimilates

The $\delta^{18}O$ of cryogenically extracted stem xylem water, as a proxy for source water, was analyzed using a thermal combustion/elementary analysis (TC/EA) system coupled to a DeltaPlusXP isotope ratio mass spectrometer (IRMS; all supplied by Thermo Fisher Scientific, Bremen, Germany) with a typical measurement precision (*SD*) of 0.2‰.

For the extraction of assimilates, a total of 60 mg ground needle material was transferred to a 2 mL reaction tube, dissolved in 1.5 mL of hot (85 °C) water and heated in a water bath at 85 °C for 30 min (Lehmann et al. 2017). Subsequently, samples were cooled down at room temperature and centrifuged (2 min, 10,000*g*), and the supernatant containing the water-soluble compounds (WSC) was transferred to a new reaction vial. An aliquot (ca. 0.6 mg) of the WSC, as a proxy for assimilates, was transferred to silver capsules, frozen at −20 °C and freeze-dried. Carbon ($\delta^{13}C$, VPDB) and oxygen ($\delta^{18}O$, VSMOW) isotope ratios were measured using a TC/EA system (vario PYRO cube, Elementar, Hanau, Germany) coupled to the abovementioned IRMS. The typical measurement precision (*SD*) was 0.3‰ for $\delta^{13}C$ values and 0.2‰ for $\delta^{18}O$ values. The ^{18}O enrichment of needle assimilates ($\Delta^{18}O_{WSC}$) above source water was calculated as the difference between the $\delta^{18}O$ of WSC and the $\delta^{18}O$ of the stem xylem water (source water) in the same tree at the same date.

Xylogenesis observations and wood anatomical measurements

Collected microcores were first embedded in paraffin and cut in 7-µm-thick transverse sections using a rotary microtome (Leica RM2245, Leica Biosystems, Nussloch, Germany). Sections were stained (with safranin and astra blue to distinguish cellulose and lignin) and permanently mounted on glass slides. Xylogenesis observations were performed on the micro-sections using an optical microscope under visible and polarized light at ×100–400 magnification to distinguish the different phases of cell development (Rossi et al. 2006). Cambial, enlarging, cell wall thickening and mature cells were visually discriminated and counted for each sample according to Cuny et al. (2019). Count data of cells in different xylogenesis phases were standardized

by the total number of cells of the previous ring (Rossi et al. 2003) using the R package CAVIAR (Rathgeber et al. 2018). All xylogenesis measurements were standardized (in %) to the total cells produced by the individual tree, to account for absolute cell production differences.

Additionally, quantitative wood anatomical analysis was used to determine cell-specific features and ring width using the increment core collected at the end of the monitoring period. For each slide, digital images were taken for the 2018 tree ring using a slide scanner (Axio Scan Z1, Zeiss, Germany). ROXAS software (von Arx and Carrer 2014) combined with Image-Pro Plus (Media Cybernetics, Rockville, MD, USA) was used to measure tracheids semi-automatically from the images (von Arx et al. 2016). Cell lumen area and cell wall thickness, together with positional information (expressed in % of the 2018 tree ring), were measured to develop tracheidograms using the R package RAPTOR (Peters et al. 2018).

Statistics

Differences in the daily mean and amplitude of climatic conditions (T_a and RH) were tested using a paired Student's *t*-test. Linear mixed-effect models with treatment ('budmoth outbreak'), time ('seasonal variations') and their interactions as fixed effects and the individual tree identification as random effect were used to test for significant differences in [Ss_{std}], [St_{std}], $\Delta^{18}O_{WSC}$ and $\delta^{13}C_{WSC}$. Differences in isotopic composition and in NSC between control and budmoth site at each sampling point were tested using a paired Student's *t*-test. For the xylogenesis and wood anatomical measurements, Student's *t*-tests were performed for each time step and cell position, respectively. The non-parametric Kruskal–Wallis test was used to examine differences between sites when there was a lack of residual normality and homogeneity. Statistical analyses were carried out using R version 3.5.1 (R Core Team 2018).

Results

Climate, crown structure and leaf trait differences

During the monitoring period, no significant differences between sites were found in daily mean and amplitude of RH ($P = 0.15$ and 0.28, respectively; Figure 1b). Mean daily T_a was slightly but significantly higher at the control site (0.8 °C, $P < 0.01$), due to the higher difference in day and night time temperature at the outbreak site (0.5 °C, $P = 0.01$). The mean daily temperature during the monitoring period (DOY 171–283) was relatively high compared to the period from 2007 to 2013 as reported by Cuny et al. (2019), (10.6 ± 3.9 °C, see Figure S1 available as Supplementary Data at *Tree Physiology* Online), with 13.4 ± 3.4 and 12.6 ± 3.5 °C for the control and budmoth site, respectively. Satellite observations revealed the impact of the larch budmoth on the effective crown damage when comparing budmoth vs. control site (Figure 1d). Despite the moderate severity of the outbreak in the studied area (trees were not completely defoliated), re-foliated trees had lower NDVI after defoliation (from the second week of July on) compared to control trees, indicating lower leaf surface area and/or lower photosynthetic activity (Figure 1d). Compared to the control plot, the new needles (collected at DOY 221) had a slightly larger surface and a markedly larger dry weight per needle, which resulted in a significantly lower SLA ($P = 0.03$; Table 3). No significant difference between sites was found for the C/N ratio of needles before and after defoliation ($P > 0.05$; results not shown).

Non-structural carbohydrates in different tissues

For all sampling dates and both sites, needles and stem phloem had the highest NSC (i.e., soluble sugars [Ss] and starch [St]) concentrations among all tissues (7.99 and 5.70% dry weight for [Ss] and 2.49 and 10.36% d.w. for [St], respectively). Average NSC concentrations in xylem tissues were below 2% in d.w. (1.44, 0.94 and 0.97% d.w. for [Ss] and 0.86, 0.67 and 1.03% d.w. for [St] in twig, stem and root xylem, respectively). Standardized needle and stem phloem NSC concentrations [Ss_{std}] were significantly lower in defoliated trees after re-foliating, compared to control trees (Figure 2). Conversely, standardized stem xylem [Ss_{std}] was higher in damaged trees during re-foliation (DOY 193) and at the end of the season (DOY 283), compared to controls. Twig and root xylem did not show significant differences in [Ss_{std}] in control vs. defoliated trees. Starch [St_{std}] concentrations showed the most severe reduction in the needles of defoliated trees after re-foliation, and these minimum levels remained unchanged until the end of the growing season (significant except in DOY 239; Figure 2). However, [St_{std}] tended to increase in trees in twig xylem (significant in DOY 186, 283) and stem phloem (significant in DOY 239) in damaged trees. Stem and root xylem did not show differences between control and budmoth trees nor did they change over time.

Seasonal carbon and oxygen isotopic composition in needle water and assimilates

The larch budmoth outbreak showed no clear effect ($P > 0.05$) on the carbon and oxygen isotopic composition of assimilates (Similar as how it is described in Figure 3). However, clear seasonal variations of ~ 1‰ in $\delta^{13}C_{WSC}$ and 4.5‰ in $\Delta^{18}O_{WSC}$ were observed ($P < 0.05$). Notably, differences in $\Delta^{18}O_{WSC}$ before the larch budmoth outbreak (DOY 171 and 172) are likely caused by strong day-to-day variations in atmospheric evaporative conditions (1.14 and 1.38 hPa for control and budmoth site, respectively).

Stem growth phenology and wood anatomy

The studied trees started cell enlargement before the sampling period and stopped by DOY 209 (Figure 4). No significant difference was found between the dynamics of the

Table 3. Summary of various needle leaf traits of larch trees from the control and budmoth site (sampled on the 9 August 2018). Mean values and standard deviation (in brackets) are given ($n = 4$).

Site	Sampled total dry weight (mg)	Sampled total leaf area (cm^2)	Needle length (cm)	Specific leaf area ($m^2\ kg^{-1}$)
Control	46.8 (22.2)	7.9 (2.7)	2.1 (0.1)	17.6 (2.5)
Budmoth	82.3 (20.6)	10.7 (2.4)	2.3 (0.2)	13.2 (1.7)

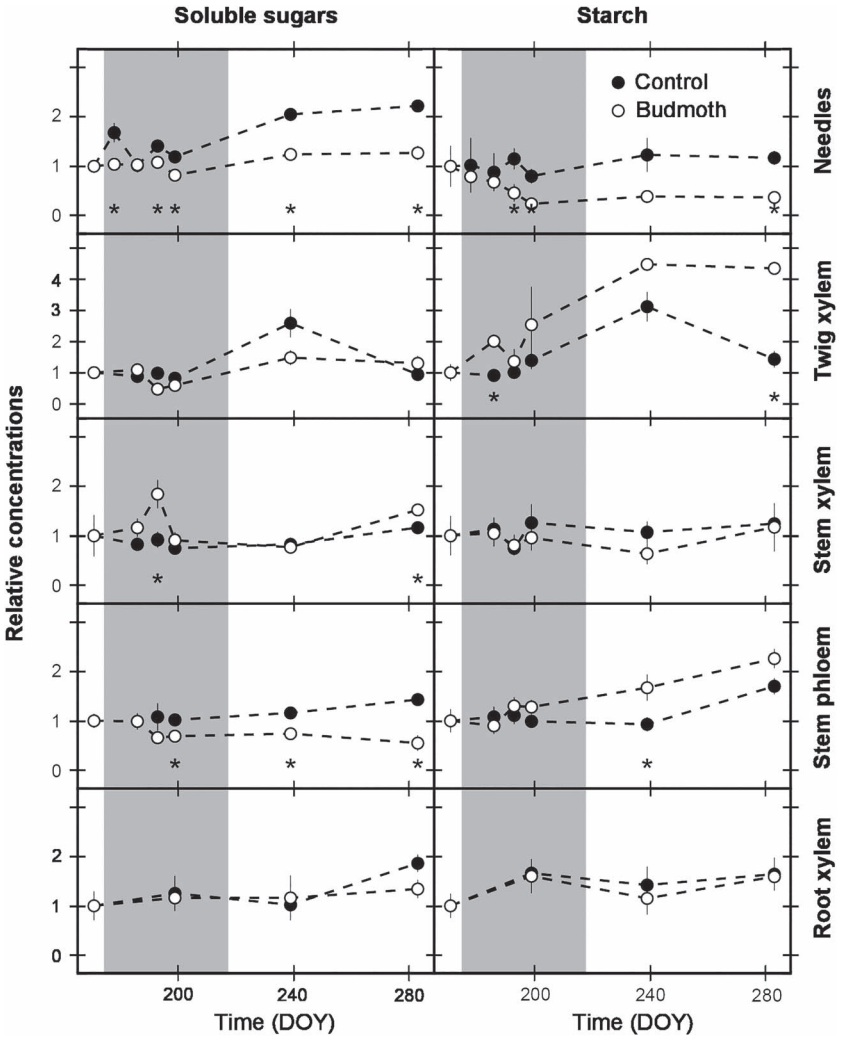

Figure 2. Seasonal non-structural carbohydrate dynamics in different larch tree tissues. Standardized NSC concentrations of mean soluble sugar and starch content for different tissues of the control and budmoth site against the day of year DOY for the 2018 growing season. All NSC values were standardized by dividing by the tree-specific initial measurements taken on 20 June 2018 (DOY 171). Stars (*) indicate significant differences between sites at that sampling date. The gray area reflects the period of visible larch budmoth defoliation. Mean values and standard errors are given ($n = 4$).

relative enlarging cell count of the control and budmoth site ($P > 0.05$). Yet, compared to literature, the cell enlargement period ceased earlier than observed in the period from 2007 to 2013 (Figure 4). Cell wall thickening of the unaffected trees at the control site started between DOY 171 and 186, when defoliation was occurring at the budmoth site, while cell wall thickening ceased earlier than expected from literature data (Figure 4). Budmoth site trees ceased cell wall thickening 17 days earlier (DOY 251) than control trees (DOY 268). In addition, the number of cells that were still in the cell wall thickening phase was significantly higher at the control site compared to the budmoth site at the end of the growing season (mean of DOY 239 and 251; $\Delta = 3$ cells when total cell production is around ~20, $P = 0.015$).

Tree-ring width measured at 2018 showed no significant difference between the control and budmoth site ($P = 0.19$; see

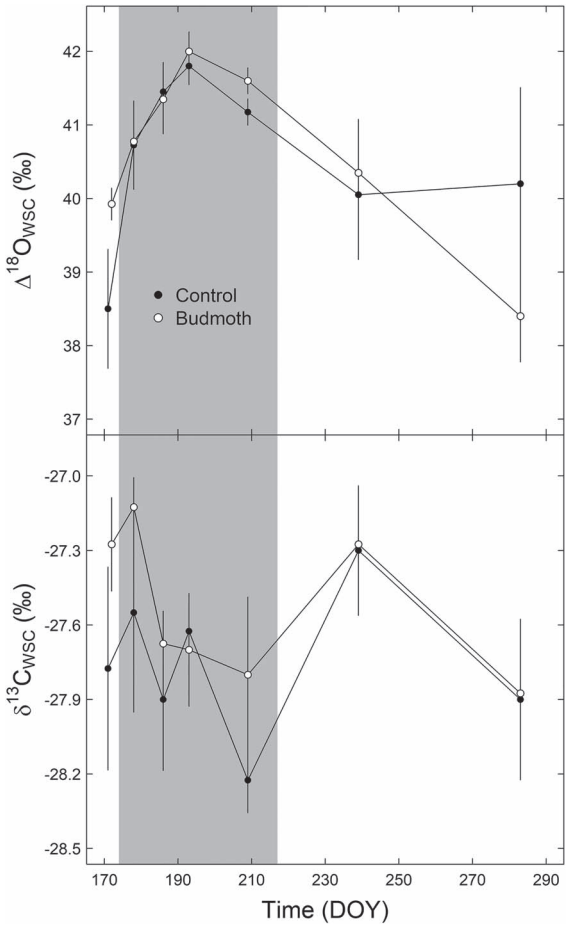

Figure 3. Seasonal isotope dynamics in larch needle assimilates. Carbon isotope ratios and oxygen isotope enrichment above source water for needle assimilates ($\delta^{13}C_{WSC}$ and $\Delta^{18}O_{WSC}$, respectively) from the control and budmoth site against the DOY for the 2018 growing season. The gray area reflects the period of visible larch budmoth defoliation. Mean values and standard errors are given ($n = 4$).

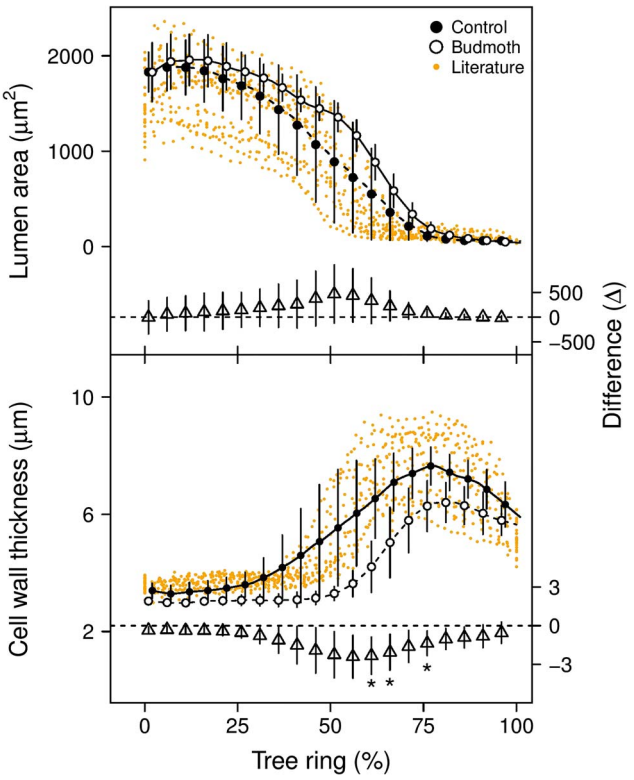

Figure 4. Lumen area and cell wall thickness composition in the 2018 tree ring of trees growing at the control and budmoth site. Orange dots represents lumen area and cell wall thickness data obtained from Cuny et al. (2019) for the period from 2007 to 2013 in trees close to the monitored sites. Data was standardized to the total cell count within 2018 of the individual tree (tree ring in %). The difference axes indicate the differences between sites at that sampling date, and stars (*) indicate significant differences. Mean and standard deviation are given ($n = 4$).

Figure S2 available as Supplementary Data at *Tree Physiology* Online). When standardizing ring width to the previous year ring width, a non-significant reduction of 19% in ring width was found for the budmoth site ($P = 0.222$). The budmoth site appeared to have a slightly higher yet non-significant larger lumen area across the tree ring of 2018 (Figure 5). Although maximum cell lumen area remains unchanged between sites ($P = 0.717$), maximum cell wall thickness appeared to be 1.24 µm lower for the budmoth site compared to the control site ($P = 0.052$). Budmoth trees showed overall thinner cell walls in 2018, with significant difference occurring in the latter part of the ring (66–76% of the tree ring; $P < 0.05$; Figure 5).

Discussion

Our multi-parameter monitoring during the 2018 larch budmoth outbreak provides for the first time a physiological explanation for the altered stem wood structure of *Larix decidua*. Despite the fact that the monitored outbreak was not as extensive as past outbreaks (Baltensweiler and Rubli 1999, Baltensweiler et al. 2008, Wermelinger et al. 2018), it revealed how insect defoliation impacts leaf physiology during and after the outbreak and how this cascades into carbohydrate storage and subsequently impacts wood formation.

Non-structural carbohydrate response to defoliation

The monitoring of the standardized seasonal non-structural carbohydrate dynamics revealed that the trees growing at the outbreak site showed a significant differentiation from the control trees in relative soluble sugar levels in both needles and phloem after the outbreak (Figure 2). The lower starch and sugar concentrations in the needles of defoliated compared to control trees cascaded solely into a reduction of soluble sugars in the phloem but not in the stem or root xylem, which confirms previous studies that found a limited impact of defoliation on NSC pools due to a strong prioritization of carbon storage (Jacquet et al. 2014, Puri et al. 2015, Weber et al. 2019). Stem and root xylem NSC were not affected by defoliation in contrast

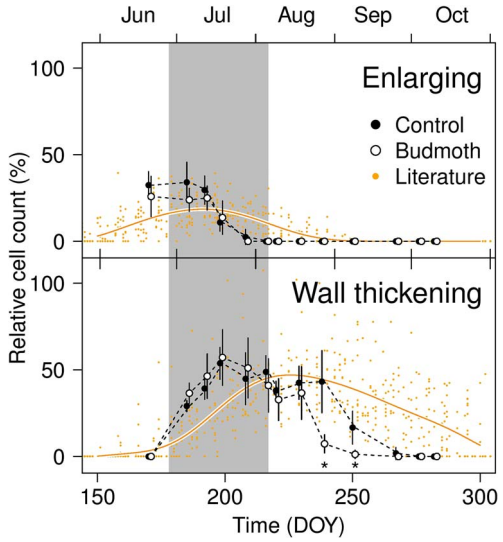

Figure 5. Relative cell count of tracheids in the enlarging (upper panel) and cell wall thickening (lower panel) phase against the DOY. Mean values and standard deviations are given ($n = 4$). Orange dots presents enlarging and cell wall thickening data obtained from Cuny et al. (2019) for the period from 2007 to 2013 in trees close to the monitored sites. The general trend of these observations is highlighted with a cubic spline (orange bold line). Relative cell count is determined by standardizing the count data to the total amount of mature cells produced by the individual tree in the current year. The gray area reflects the period of larch budmoth defoliation. Stars (*) indicate significant differences between sites at that sampling date.

to findings from Li et al. (2002), where carbon reserves were depleted in those tissues of evergreen *Pinus cembra* after defoliated. This could be due to the difference between deciduous *L. decidua* and evergreen conifers, which likely are better adapted and have stricter control over their carbon storage pools due to the difference in the leaf economic spectrum (see Wright et al. 2004), where deciduous trees require more carbon for annual re-foliation. The trees at the outbreak site, however, showed a steeper increase in standardized starch concentrations in stem phloem and particularly in twig xylem compared to the control trees (Figure 2). Thus, NSC content in woody tissues remained generally unchanged or increased due to the budmoth outbreak, indicating that the affected trees prioritize maintenance of their NSC content and thus carbon availability after stress or that carbon pools are plentiful so that re-foliation does not affect previous NSC pools.

With normal seasonal patterns, sugars are increasingly made available within the cambium for cell wall thickening (as observed in *L. decidua* in Simard et al. 2013). Yet, the reduced carbon supply due to reduced leaf area and stable NSC content with prioritization for carbon storage in some tissues could explain the earlier halt of cell wall thickening in our study. The impact of lower carbon availability at the cambium has been studied by altering phloem transport, where the cut-off of sugars due to girdling had a strong downregulating effect on cell wall thickness (shown in *Picea abies* in Winkler and Oberhuber 2017). These findings are also supported by artificial defoliation experiments (e.g., Wiley et al. 2016) which show that defoliation by the pine processionary moth on *Pinus nigra* tended to cause an increase in NSC concentrations while downregulating growth (Palacio et al. 2012). For our high-elevation *L. decidua* trees, these results indicate that despite the availability of plentiful carbon for growth (as hypothesized by Körner 2003, contrasting Handa et al. 2005), the *L. decidua* trees prioritize re-foliation and the replenishment of their storage. The priority for carbon investment in re-foliation is likely enhanced as needles growing after defoliation have been shown to have a more carbon-demanding lignin content, supposedly as a defense against future herbivory (Asshoff and Hättenschwiler 2006). The priority for stored carbon could be an adaptation to the colder environmental conditions that require sugars within the stem (e.g., raffinose and pinitol) at the end of the growing season to facilitate the protection against frost-induced damages (Simard et al. 2013, Lintunen et al. 2016). In combination with previous findings, our results suggest a universal tree physiological response to various stressors like defoliation, cold temperatures or drought, where cambial activity and growth are strongly downregulated during stress while attempting to maintain photosynthesis, storage and respiration (which was suggested for drought stress by McDowell 2011).

Absence of leaf physiological differences in regrown needles after budmoth outbreak

The unaltered ratio of C/N after defoliation agrees with Asshoff and Hättenschwiler (2006) who only found reductions in N the year after defoliation. Moreover, the specific leaf area was lower at the outbreak site (Table 3), suggesting that the trees produced more resource-intensive needles per unit leaf area. However, results from the carbon and oxygen isotope measurements of needle assimilates (Figure 3) did not provide clear evidence for a leaf functional response to the larch budmoth outbreak. Our results are therefore going along with isotope analyses of annual tree rings on the same site (Kress et al. 2009), which also observed no clear influence of the larch budmoth outbreaks over several decades/centuries, although fluctuation in density and tree-ring growth were observed. The $\delta^{13}C_{WSC}$ and $\Delta^{18}O_{WSC}$ values indicate that neither photosynthetic assimilation rates nor stomatal conductance was different between control needles and newly grown needles in budmoth-affected trees (Scheidegger et al. 2000). These results highlight that *L. decidua* does not increase photosynthetic capacity, as found in other species (e.g., Reich 1992, Eyles et al. 2011), emphasizing the species-specific strategy of altering leaf physiology after a defoliation (Piper and Fajardo 2014). Moreover, the strong seasonality in $\Delta^{18}O_{WSC}$ values in both treatments are explained by the changes in vapour pressure deficit (VPD) during the growing season (Kahmen et al. 2011,

Song et al. 2013), which was also previously observed at the same site in phloem organic matter (Treydte et al. 2014). This shows that the affected trees were able to maintain the physiological functionality of newly grown needles throughout the growing season, although environmental conditions during regrowth were different compared to those in spring (i.e., higher temperature and VPD) when the needles of control trees emerged.

Direct wood structural responses to the outbreak

Despite the fact that up to ~80% of the crown of the trees growing at the outbreak site was defoliated (Table 1), causing a reduction in the satellite derived NDVI (Figure 1d), no significant difference was found between the ring widths measured at the budmoth vs. control site (see Figure S2 available as Supplementary Data at *Tree Physiology* Online). These results contrast with past studies which successfully used ring width as a proxy for detecting defoliation events in the past, with narrow rings indicating an outbreak (Rolland et al. 2001, Büntgen et al. 2009, Hartl-Meier et al. 2017). We hypothesize that this discrepancy is present due to the timing of the outbreak, as maximum cell enlargement rates were already reached in this study causing a large part of the ring to be formed by the time the outbreak started (end of June; Figure 5). This is supported by the fact that 2018 was relatively warm (see Figure S1 available as Supplementary Data at *Tree Physiology* Online) which is known to increase growth rates at these elevations and promote an earlier cambial onset (Frank and Esper 2005, Rossi et al. 2008, Cuny et al. 2019). In addition, 2018 was an extremely dry year in Switzerland, with high temperatures and below-average precipitation in the spring and summer months (MeteoSchweiz 2018, Liechti et al. 2019). The effects of dry conditions likely explain the decrease in NDVI observed at both the control and budmoth sites in June and could confound the differences between the budmoth and control sites. Alternatively, the impact of this particular outbreak on ring width could become more pronounced in the first years after the outbreak (see Baltensweiler et al. 2008, Peters et al. 2017), as the NSC reduction in the current year was not sufficient to reduce the osmotic pressure and subsequently reduce cambial division and cell enlargement, which is also driven by water availability (Cabon et al. 2019, Cabon et al. 2020, De Schepper and Steppe 2010). Notwithstanding, the defoliation intensity of the outbreak could still have been moderate, as Baltensweiler and Rubli (1999) have reported events where defoliation occurred during multiple years. These findings question whether ring width is a proxy capable of detecting outbreak years of lesser intensity.

However, clear signs of the outbreak are recorded in the wood structure. The observations of wood formation revealed that cell wall thickening responded within the outbreak year, halting 17 days earlier at the budmoth compared to the control site, which is among the earliest occurrences of a stop of cell wall thickening monitored at the approximate elevation (Cuny et al. 2019; Figure 4). Additionally, the outbreak appeared to reduce the number of cells in the wall thickening phase after mid-August (DOY = 230; Figure 2), which resulted in significant thinner cell walls and thinner latewood at the budmoth site (Figure 5), characteristic for a budmoth ring (Rolland et al. 2001). The relatively early halt of enlargement and cell wall thickening at both sites in 2018 compared to previous observations (Cuny et al. 2019) could be attributed to the warm and dry conditions which is known to halt the wood formation processes (e.g., Vieira et al. 2014). Yet, the discrepancy in response of cell enlargement and wall thickening, where the budmoth site only differed in wall thickening, highlights the decoupling between radial growth and carbon allocation in cell walls (Cuny et al. 2015, 2019). This discrepancy is also highlighted by the longer climatic response window of cell wall thickness compared to lumen diameter (as shown for climatic response of *Picea abies* in Castagneri et al. 2017). Notwithstanding, the fact that cell wall thickness responded within the year of outbreak confirms past studies which detected outbreaks using latewood density and width (e.g., Esper et al. 2007, Arbellay et al. 2018). This observed hampering of carbon investment into thick cell walls is consistent with experimental studies, which showed a strong downregulation of carbon allocation in woody biomass during defoliation (e.g., Schmid et al. 2017) and as a consequence could reduce mechanical stability (Hillabrand et al. 2019).

Is wood formation limited by carbon availability after the outbreak?

Our results present the first physiological monitoring of the intra-annual impact of a larch budmoth outbreak on the structure and function of *L. decidua*. We hypothesized that the temporal lack of carbon input due to defoliation would be compensated by either (H1) increasing photosynthetic capacity of the regrown needles, stabilizing NSC concentrations, while downregulating wood formation processes, or, in contrast, through (H2) an unaltered leaf physiology in regrown needles, reducing NSC levels and retarding wood formation. Our finding strongly supports the idea that needle growth and functioning is a high priority for larch budmoth affected trees, yet no alteration within the physiology of needles was observed, rejecting H1. We, however, only partially confirm H2, as *L. decidua* still seems to prioritize carbon storage over growth after a defoliation event, where starch levels are constant or increase in woody tissues throughout the season in budmoth affected trees. This reveals that NSC present within the trees is not the main factor regulating or limiting cambial activity (e.g., Hoch et al. 2002, Simard et al. 2013). The observed natural reduction in carbon availability due to defoliation and the subsequent response of internal carbon allocation reveal that there is a need to rethink the carbon source–sink paradigm (e.g., Friend

et al. 2019), as it appears to be a stronger downregulation of wood formation processes while carbon is still available (Körner 2015).

The absence of extensive budmoth outbreaks after the early 1980s has prevented the detailed assessment of the physiological response of *L. decidua* to an outbreak. The absence of outbreaks has been attributed to changes in forest structure and species composition (Battipaglia et al. 2014, Hartl-Meier et al. 2017); changes in nitrogen, water, starch and sugar content of foliage (Turchin et al. 2003, Asshoff and Hättenschwiler 2006); and climate (Johnson et al. 2010, Iyengar et al. 2016). The reason for its return in 2018 is unclear, yet the population growth dynamics of the budmoth appeared to continue its ~9-year cyclic pattern after the absence of visible defoliation events since the 1980s (e.g., Esper et al. 2007, Wermelinger et al. 2018, Büntgen et al. 2020). The pattern of lacking outbreaks and the recent resurrection occurred throughout the alpine arch, hinting towards the important role of large-scale climate effects in driving the budmoth population dynamics (Turchin et al. 2003). A recent study by Büntgen et al. (2020) attributes the reoccurrence to cold European winters due to the persistent negative phase of the North Atlantic Oscillation, which they hypothesize to have caused a (i) reduction in egg mortality due to lower energy consumption through the extended diapause, (ii) phenological synchrony between egg hatching and needle growth and (iii) shift of the outbreak epicenter to subalpine forests with higher host abundance. Due to the sudden return of the outbreak, we were unable to capture climatic conditions and wood formation dynamics at the start of the growing season, which could have provided more insights into the annual carbon allocation patterns. Additionally, monitoring of these multiple measurements should be continued to further explain lag effects on biomass accumulation, which have been observed up to 7 years after the outbreak (e.g., Peters et al. 2017). Although relative difference and seasonal dynamics of wood formation processes (i.e., cell enlargement and cell wall thickening) can be assessed (also due to the extensive reference dataset; Cuny et al. 2019), differences in absolute wood anatomical properties, carbon availability and growth might be influenced by differences in stand density (Table 1), tree size and local climatic conditions (see Figure S1 available as Supplementary Data at *Tree Physiology* Online) between control and budmoth site. Additionally, while relative changes in NSC concentrations were assessed, it should be noted that absolute NSC concentrations are difficult to interpret due to the difference in growing conditions between sites. Moreover, the high temperature and below-average precipitation in summer of 2018 could have an interacting effect with defoliation on the wood structure, which is difficult to disentangle. Future and long-term investigations and experimental manipulations are thus needed to contribute to the better understanding of the interactions between insect outbreaks and internal carbohydrate allocation of trees and to assess the future fate of the forest sink capacity under changing outbreak regimes (e.g., Bale et al. 2002, McMahon et al. 2010, Medvigy et al. 2012).

Conclusion

Our study on the direct physiological response of subalpine *L. decidua* to a larch budmoth outbreak provides novel insights into the processes forming ring-width structures, which is important for a reliable reconstruction of outbreak dynamics over millennia. It sheds light on the process of tree carbon allocation priorities in time of reduced carbon assimilation. Trees defoliated during a budmoth outbreak appeared to downregulate cell wall thickening, resulting in a wood structure with thinner cell walls and latewood, while not mobilizing longer-term starch storage or adjusting leaf physiology to increase carbon available for wood formation. These observations suggest that carbon dynamics and its storage have to be considered when assessing cambial activity and the subsequent carbon allocation into wood, not only for insect outbreak events but potentially many other stressors, relevant for addressing the carbon sink capacity of forests.

Supplementary data

Supplementary Data for this article are available at *Tree Physiology* Online.

Acknowledgments

We thank Roman Zweifel for his aid in the field and lab work performed at the Lötschental transect. We also would like to thank Andreas Rigling, Arthur Gessler, Flurin Babst and Stefan Klesse for discussion.

Conflict of interest

The authors declare that they have no conflict of interest.

Funding

The work was supported by the Swiss National Science Foundation (SNF) Early Postdoc.Mobility (grant P2BSP3_184475), SNF LOTFOR (grant 150205), SNF CLIMWOOD (grant 160077), SNF Ambizione (grant PZ00P2_179978) and Fundación Ramón Areces.

References

Anderegg WRL, Hicke JA, Fisher RA et al. (2015) Tree mortality from drought, insects, and their interactions in a changing climate. New Phytol 208:674–683.

Arbellay E, Jarvis I, Chavardès RD, Daniels LD, Stoffel M (2018) Tree-ring proxies of larch bud moth defoliation: latewood width and

blue intensity are more precise than tree-ring width. Tree Physiol 38:1237–1245.

Asshoff R, Hättenschwiler S (2006) Changes in needle quality and larch bud moth performance in response to CO_2 enrichment and defoliation of treeline larches. Ecol Entomol 31:84–90.

Bale JS, Masters GJ, Hodkinson ID et al. (2002) Herbivory in global climate change research: direct effects of rising temperature on insect herbivores. Glob Chang Biol 8:1–16.

Baltensweiler W, Fischlin A (1988) The larch bud moth in the Alps. In: Berryman AA (ed) Dynamics of forest insect populations. Plenum Press, New York, pp 331–351.

Baltensweiler W, Rubli D (1999) Dispersal: an important driving force of the cyclic population dynamics of the larch bud moth, *Zeiraphera diniana* Gn. For Snow Landscape Res 74:1–153.

Baltensweiler W, Weber UM, Cherubini P (2008) Tracing the influence of larch-bud-moth insect outbreaks and weather conditions on larch tree-ring growth in Engadine (Switzerland). Oikos 117:161–172.

Battipaglia G, Büntgen U, McCloskey S, Blarquez O, Denis N, Paradis L, Brossier B, Fournier T, Carcaillet C (2014) Long-term effects of climate and land-use change on larch budmoth outbreaks in the French alps. Clim Res 62:1–14.

Benz A (1974) Negative Rückkoppelungen durch Raum- und Nahrungskonkurrenz sowie zyklische Veränderung der Nahrungsgrundlage als Regelprinzip in der Populationsdynamik des Grauen Lärchenwicklers, Zeiraphera diniana (Guenée) (Lep., Tortricidae). Z Ang Entomol 76:196–228.

Büntgen U, Frank D, Liebhold A et al. (2009) Three centuries of insect outbreaks across the European Alps. New Phytol 182:929–941.

Büntgen U, Liebhold A, Nievergelt D et al. (2020) Return of the moth: rethinking the effect of climate on insect outbreaks. Oecologia 192:543–552.

Cabon A, Fernández-de-Uña L, Gea-Izquierdo G, Meinzer FC, Woodruff DR, Martínez-Vilalta J, De Cáceres M (2019) Water potential control of turgor-driven tracheid enlargement in scots pine at its xeric distribution edge. New Phytol 225:209–221.

Cabon A, Peters RL, Fonti P, Martinez-Villalta J, De Cáceres M, Martínez-Vilalta J, De Cáceres M (2020) Temperature and water potential co-limit stem cambial activity along a steep elevational gradient.. New Phytologist 226:1325–1340. doi: 10.1111/nph.16456.

Castagneri D, Fonti P, von Arx G, Carrer M (2017) How does climate influence xylem morphogenesis over the growing season? Insights from long-term intra-ring anatomy in *Picea abies*. Ann Bot 119:1011–1020.

Castagneri D, Prendin AL, Peters RL, Carrer M, von Arx G, Fonti P (2020) Long-term impacts of defoliator outbreaks on larch xylem structure and wood biomass. Frontiers in Plant Sciences 11:1078.

Cuny HE, Fonti P, Rathgeber CBK, von Arx G, Peters RL, Frank DC (2019) Couplings in cell differentiation kinetics mitigate air temperature influence on conifer wood anatomy. Plant Cell Environ 42:1222–1232.

Cuny HE, Rathgeber CBK, Frank D, Fonti P, Fournier M (2014) Kinetics of tracheid development explain conifer tree-ring structure. New Phytol 203:1231–1241.

Cuny HE, Rathgeber CBK, Frank D et al. (2015) Woody biomass production lags stem-girth increase by over one month in coniferous forests. Nat Plants 1:1–6.

De Schepper V, Steppe K (2010) Development and verification of a water and sugar transport model using measured stem diameter variations. J Exp Bot 61:2083–2099.

Esper J, Buntgen U, Frank DC, Nievergelt D, Liebhold A (2007) 1200 years of regular outbreaks in alpine insects. Proc R Soc B Biol Sci 274:671–679.

Eyles A, Smith D, Pinkard EA, Smith I, Corkrey R, Elms S, Beadle C, Mohammed C (2011) Photosynthetic responses of field-grown *Pinus radiata* trees to artificial and aphid-induced defoliation. Tree Physiol 31:592–603.

Foster JR (2017) Xylem traits, leaf longevity and growth phenology predict growth and mortality response to defoliation in northern temperate forests. Tree Physiol 37:1151–1165.

Frank D, Esper J (2005) Characterization and climate response patterns of a high-elevation, multi-species tree-ring network in the European Alps. Dendrochronologia 22:107–121.

Friend AD, Eckes-Shephard AH, Fonti P, Rademacher TT, Rathgeber CBK, Richardson AD, Turton RH (2019) On the need to consider wood formation processes in global vegetation models and a suggested approach. Ann For Sci 76:49.

Galiano L, Martínez-Vilalta J, Lloret F (2011) Carbon reserves and canopy defoliation determine the recovery of scots pine 4yr after a drought episode. New Phytol 190:750–759.

Giron D, Dubreuil G, Bennett A et al. (2018) Promises and challenges in insect–plant interactions. Entomol Exp Appl 166: 319–343.

Gleason SM, Ares A (2004) Photosynthesis, carbohydrate storage and survival of a native and an introduced tree species in relation to light and defoliation. Tree Physiol 24:1087–1097.

Handa IT, Körner C, Hättenschwiler S (2005) A test of the treeline carbon limitation hypothesis by in situ CO_2 enrichment and defoliation. Ecology 86:1288–1300.

Hartl-Meier C, Esper J, Liebhold A, Konter O, Rothe A, Büntgen U (2017) Effects of host abundance on larch budmoth outbreaks in the European Alps. Agric For Entomol 19:376–387.

Hartmann F, Rathgeber C, Fournier M, Moulia B (2017) Modelling wood formation and structure: power and limits of a morphogenetic gradient in controlling xylem cell proliferation and growth. Ann For Sci 74:1–15.

Hillabrand RM, Hacke UG, Lieffers VJ (2019) Defoliation constrains xylem and phloem functionality. Tree Physiol 39:1–29.

Hoch G, Popp M, Körner C (2002) Altitudinal increase of mobile carbon pools in *Pinus cembra* suggests sink limitation of growth at the Swiss treeline. Oikos 3:361–374.

Iyengar SV, Balakrishnan J, Kurths J (2016) Impact of climate change on larch budmoth cyclic outbreaks. Sci Rep 6:27845.

Jacquet JS, Bosc A, O'Grady A, Jactel H (2014) Combined effects of defoliation and water stress on pine growth and non-structural carbohydrates. Tree Physiol 34:367–376.

Johnson DM, Bjørnstad ON, Liebhold AM (2004) Landscape geometry and travelling waves in the larch budmoth. Ecol Lett 7:967–974.

Johnson DM, Buntgen U, Frank DC, Kausrud K, Haynes KJ, Liebhold AM, Esper J, Stenseth NC (2010) Climatic warming disrupts recurrent alpine insect outbreaks. Proc Natl Acad Sci 107: 20576–20581.

Kahmen A, Sachse D, Arndt SK, Tu KP, Farrington H, Vitousek PM, Dawsona TE (2011) Cellulose $\delta^{18}O$ is an index of leaf-to-air vapor pressure difference (VPD) in tropical plants. Proc Natl Acad Sci USA 108:1981–1986.

King G, Fonti P, Nievergelt D, Büntgen U, Frank D (2013) Climatic drivers of hourly to yearly tree radius variations along a 6°C natural warming gradient. Agric For Meteorol 168:36–46.

Körner C (2003) Carbon limitation in trees. J Ecol 91:4–17.

Körner C (2015) Paradigm shift in plant growth control. Plant Biol 25:107–114.

Kress A, Saurer M, Büntgen U, Treydte KS, Bugmann H, Siegwolf RTW (2009) Summer temperature dependency of larch budmoth outbreaks revealed by alpine tree-ring isotope chronologies. Oecologia 160:353–365.

Lehmann MM, Gamarra B, Kahmen A, Siegwolf RTW, Saurer M (2017) Oxygen isotope fractionations across individual leaf carbohydrates in grass and tree species. Plant Cell Environ 40:1658–1670.

Lehmann MM, Goldsmith GR, Schmid L, Gessler A, Saurer M, Siegwolf RTW (2018) The effect of ^{18}O-labelled water vapour on the oxygen isotope ratio of water and assimilates in plants at high humidity. New Phytol 217:105–116.

Li M, Hoch G, Körner C (2002) Source/sink removal affects mobile carbohydrates in *Pinus cembra* at the Swiss treeline. Trees-Struct Funct 16:331–337.

Liechti K, Barben M, Zappa M (2019) Wasserhaushalt der Schweiz im Jahr 2018. Einordnung und Besonderheiten. Wasser Energie Luft 111:93–94.

Lintunen A, Paljakka T, Jyske T et al. (2016) Osmolality and non-structural carbohydrate composition in the secondary phloem of trees across a latitudinal gradient in Europe. Front Plant Sci 7.

McDowell N, Pockman WT, Allen CD et al. (2008) Mechanisms of plant survival and mortality during drought: why do some plants survive while others succumb to drought? New Phytol 178:719–739.

McDowell NG (2011) Mechanisms linking drought, hydraulics, carbon metabolism, and vegetation mortality. Plant Physiol 155: 1051–1059.

McMahon SM, Parker GG, Miller DR (2010) Evidence for a recent increase in forest growth. Proc Natl Acad Sci 107:3611–3615.

Medvigy D, Clark KL, Skowronski NS, Schäfer KVR (2012) Simulated impacts of insect defoliation on forest carbon dynamics. Environ Res Lett 7:45703.

MeteoSchweiz (2018) Klimabulletin Sommer 2018, Zürich. https://www.meteoschweiz.admin.ch/content/dam/meteoswiss/de/service-und-publikationen/Publikationen/doc/2018_JJA_d.pdf.

Palacio S, Hernández R, Maestro-Martínez M, Camarero JJ (2012) Fast replenishment of initial carbon stores after defoliation by the pine processionary moth and its relationship to the re-growth ability of trees. Trees-Struct Funct 26:1627–1640.

Peters RL, Balanzategui D, Hurley AG, von Arx G, Prendin AL, Cuny HE, Björklund J, Frank DC, Fonti P (2018) RAPTOR: row and position tracheid organizer in R. Dendrochronologia 47:10–16.

Peters RL, Klesse S, Fonti P, Frank DC (2017) Contribution of climate vs. larch budmoth outbreaks in regulating biomass accumulation in high-elevation forests. For Ecol Manag 401:147–158.

Peters RL, Speich M, Pappas C et al. (2019) Contrasting stomatal sensitivity to temperature and soil drought in mature alpine conifers. Plant Cell Environ 42:1–16.

Piper FI, Fajardo A (2014) Foliar habit, tolerance to defoliation and their link to carbon and nitrogen storage. J Ecol 102:1101–1111.

Poyatos R, Aguadé D, Galiano L, Mencuccini M, Martínez-Vilalta J (2013) Drought-induced defoliation and long periods of near-zero gas exchange play a key role in accentuating metabolic decline of scots pine. New Phytol 200:388–401.

Pureswaran DS, Roques A, Battisti A (2018) Forest insects and climate change. Curr For Rep 4:35–50.

Puri E, Hoch G, Körner C (2015) Defoliation reduces growth but not carbon reserves in Mediterranean *Pinus pinaster* trees. Trees 29:1187–1196.

R Core Team (2018) R: A language and environment for statistical computing. R Foundation for Statistical Computing, Vienna, Austria https://www.R-project.org/.

Rademacher TT, Basler D, Eckes-Shephard AH, Fonti P, Friend AD, Le Moine J, Richardson AD (2019) Using direct phloem transport manipulation to advance understanding of carbon dynamics in forest trees. Frontier For Glob Change 2. https://www.frontiersin.org/articles/10.3389/fpls.2016.00726/full.

Rathgeber CBK, Cuny HE, Fonti P (2016) Biological basis of tree-ring formation: a crash course. Front Plant Sci 7:1–7.

Rathgeber CBK, Santenoise P, Cuny HE (2018) CAVIAR: an R package for checking, displaying and processing wood-formation-monitoring data. Tree Physiol 38:1246–1260.

Reich PB, Walters MB, Krause SC, Vanderklein DW, Raffs KF, Tabone T (1993) Growth, nutrition and gas exchange of *Pinus resinosa* following artificial defoliation. Trees 7:67–77.

Rolland C, Baltensweiler W, Petitcolas V (2001) The potential for using *Larix decidua* ring widths in reconstructions of larch budmoth (*Zeiraphera diniana*) outbreak history: dendrochronological estimates compared with insect surveys. Trees-Struct Funct 15: 414–424.

Rossi S, Deslauriers A, Anfodillo T (2006) Assessment of cambial activity and xylogenesis by microsampling tree species: an example at the alpine timberline. IAWA J 27:383–394.

Rossi S, Deslauriers A, Griçar J et al. (2008) Critical temperatures for xylogenesis in conifers of cold climates. Glob Ecol Biogeogr 17:696–707.

Rossi S, Deslauriers A, Morin H (2003) Application of the Gompertz equation for the study of xylem cell development. Dendrochronologia 21:33–39.

Scheidegger Y, Saurer M, Bahn M, Siegwolf R (2000) Linking stable oxygen and carbon isotopes with stomatal conductance and photosynthetic capacity: a conceptual model. Oecologia 125:350–357.

Schmid S, Palacio S, Hoch G (2017) Growth reduction after defoliation is independent of CO_2 supply in deciduous and evergreen young oaks. New Phytol 214:1479–1490.

Schönbeck L, Gessler A, Hoch G, McDowell NG, Rigling A, Schaub M, Li MH (2018) Homeostatic levels of nonstructural carbohydrates after 13 yr of drought and irrigation in *Pinus sylvestris*. New Phytol 219:1314–1324.

Simard S, Giovannelli A, Treydte K, Traversi ML, King GM, Frank D, Fonti P (2013) Intra-annual dynamics of non-structural carbohydrates in the cambium of mature conifer trees reflects radial growth demands. Tree Physiol 33:913–923.

Simard S, Morin H, Krause C, Buhay WM, Treydte K (2012) Tree-ring widths and isotopes of artificially defoliated balsam firs: a simulation of spruce budworm outbreaks in Eastern Canada. Environ Exp Bot 81:44–54.

Song X, Barbour MM, Farquhar GD, Vann DR, Helliker BR (2013) Transpiration rate relates to within- and across-species variations in effective path length in a leaf water model of oxygen isotope enrichment. Plant Cell Environ 36:1338–1351.

Treydte K, Boda S, Pannatier EG et al. (2014) Seasonal transfer of oxygen isotopes from precipitation and soil to the tree ring: source water versus needle water enrichment. New Phytol 202: 772–783.

Turchin P, Wood SN, Ellner SP, Kendall BE, Murdoch WW, Fischlin A, Casas J, McCauley E, Briggs CJ (2003) Dynamical effects of plant quality and parasitism on larch budmoth. Ecology 84:1207–1214.

Vieira J, Rossi S, Campelo F, Freitas H, Nabais C (2014) Xylogenesis of *Pinus pinaster* under a Mediterranean climate. Ann For Sci 71: 71–80.

von Arx G, Crivellaro A, Prendin AL, Čufar K, Carrer M (2016) Quantitative wood anatomy-practical guidelines. Front Plant Sci 7:1–13.

von Arx G, Carrer M (2014) Roxas-A new tool to build centuries-long tracheid-lumen chronologies in conifers. Dendrochronologia 32:290–293.

Weber R, Gessler A, Hoch G (2019) High carbon storage in carbon-limited trees. New Phytol 222:171–182.

Weigt RB, Streit K, Saurer M, Siegwolf RTW (2018) The influence of increasing temperature and CO_2 concentration on recent growth of old-growth larch: contrasting responses at leaf and stem processes derived from tree-ring width and stable isotopes. Tree Physiol 38:706–720.

Wermelinger B, Forster B, Nievergelt D (2018) Cycles and importance of the larch budmoth. WSL Fact Sheet 61:1–12. https://www.dora.lib4ri.ch/wsl/islandora/object/wsl:18706.

Wiley E, Casper BB, Helliker BR (2016) Recovery following defoliation involves shifts in allocation that favour storage and reproduction over radial growth in black oak. J Ecol 105:412–424.

Wiley E, Huepenbecker S, Casper BB, Helliker BR (2013) The effects of defoliation on carbon allocation: can carbon limitation reduce growth in favour of storage? Tree Physiol 33:1216–1228.

Winkler A, Oberhuber W (2017) Cambial response of Norway spruce to modified carbon availability by phloem girdling. Tree Physiol 37:1527–1535.

Wright IJ, Reich PB, Westoby M et al. (2004) he worldwide leaf economics spectrum. Tree Physiol 428:821–827.